Thermal remixing of phase-separated states in two-component bosonic condensates

2015 New J. Phys. 17 103040

(http://iopscience.iop.org/1367-2630/17/10/103040)

New Journal of Physics
The open access journal at the forefront of physics

Deutsche Physikalische Gesellschaft DPG
IOP Institute of Physics

Published in partnership with: Deutsche Physikalische Gesellschaft and the Institute of Physics

OPEN ACCESS

RECEIVED
25 June 2015

REVISED
10 September 2015

ACCEPTED FOR PUBLICATION
14 September 2015

PUBLISHED
19 October 2015

PAPER

Thermal remixing of phase-separated states in two-component bosonic condensates

Peder Notto Galteland[1], **Egor Babaev**[2] **and Asle Sudbø**[1,3]

[1] Department of Physics, Norwegian University of Science and Technology, N-7491 Trondheim, Norway
[2] Department of Theoretical Physics, The Royal Institute of Technology, 10691 Stockholm, Sweden
[3] Author to whom any correspondence should be addressed.

E-mail: asle.sudbo@ntnu.no

Keywords: Bose–Einstein condensates, phase separation, thermal remixing, phase transitions, competing orders

Abstract

We consider a two-component interacting bosonic condensate with dominating intra-species repulsive density–density interactions. We study the phase diagram of the system at finite temperature with rotation, using large-scale Monte Carlo simulations of a two-component Ginzburg–Landau model of the system. In the presence of rotation, the system features a competition between long-range vortex–vortex interactions and short-range density–density interactions. This leads to a rotation-driven 'mixing' phase transition in a spatially inhomogeneous state with a broken U(1) symmetry. Thermal fluctuations in this state lead to nematic two-component sheets of vortex liquids. At sufficiently strong inter-component interaction, we find that the superfluid and $\mathbb{Z}_2$ phase transitions split. This results in the formation of an intermediate state which breaks only $\mathbb{Z}_2$ symmetry. It represents two phase separated normal fluids with a difference in their densities.

1. Introduction

Multi-component phase-coherent condensates, such as multi-component superconductors and Bose–Einstein condensates (BECs), have proven to be a rich ground for exploring quantum phenomena in condensed matter physics. In particular, BECs serve as a highly useful synthetic model systems for a wide variety of real condensed matter systems, due to their tunable interactions using magnetic and optical Feshbach-resonances. By creating mixtures of the same boson in different hyperfine states, one effectively creates multicomponent condensates [1–4]. Furthermore, by using crossed lasers, one may set up lattice model systems with a vast combinations of intersite hopping matrix elements, as well as intrasite interactions, both intra- and interspecies [5–10]. This means that these model systems, apart from being interesting in their own right, emulate various aspects of a plethora of condensed matter systems of great current interest, such as multicomponent superconductors, Mott-insulators, and even topologically nontrivial band insulators. The latter follows from the recent realization of synthetic spin-orbit couplings in such condensates [11–13]. Of particular interest is the physics of these systems in the strong coupling regime.

BECs with two components of the order parameter (two species of particles) represent a first step away from ordinary single-component condensates. This extension opens up a whole vista of physics which has no counterpart compared to single-component condensates, due to the wide variety of interspecies couplings that may be generated. Thus, these systems display physics which is beyond what is ordinarily seen in condensed matter systems, but may nevertheless serve as useful model systems for future artificially engineered condensed matter systems. As such, it is of interest to chart their physical properties to the maximum extent over a wide range of parameters.

The parameter range where inter-component density–density interactions exceed intra-component density–density interactions signals the onset of immiscibility, or phase separation, of the two components. Numerical works solving the Gross–Pitaevskii ground-state equations have also found interesting vortex lattices in this regime [14–16, 19–24]. The effect of the repulsive inter-component density–density interactions

overpowering the intra-component interactions causes the condensate to form intertwined sheets of vortices when the condensate is subject to rotation [25]. The condition for immiscibility is readily realized experimentally, using magnetic and optical Feschbach resonances [16, 26]. Several works have also focused on the critical properties of the rotation-free model using RG, mean-field and quantum Monte Carlo simulations [17, 18].

In the present paper, we focus on the regime of density–density interactions where the inter-component interactions are larger than the intra-component interactions. This regime is qualitatively different from the case in which the intra-component interactions dominate, in that immiscibility (phase-separation) of the condensate components sets in. This leads to density-modulated non-uniform ground states. Previous works have studied the effect of an inter-component density–density interaction on the rotation-induced non-homogeneous ground states. These works were mostly limited to two spatial dimensions solving the Gross–Pitaevskii ground-state equations [14–16, 19–25], although certain aspects of the three-dimensional case were also studied at the mean-field level [15, 24]. Here, we consider the case of three dimensions, taking fully into account the thermal density- and phase-fluctuation of the condensate ordering fields.

2. Definitions

2.1. Model

We consider a general Ginzburg–Landau (GL) model of an N-component BECs, which in the thermodynamic limit is defined as

$$\mathcal{Z} = \int \prod_{i}^{N} \mathcal{D}\psi_i \mathrm{e}^{-\beta H}, \tag{1}$$

where

$$H = \int \mathrm{d}^3 r \left[\sum_{i=1}^{N} \sum_{\mu=1}^{3} \frac{\hbar^2}{2m_i} \left| \left(\partial_\mu - \mathrm{i}\frac{2\pi}{\Phi_0} A_\mu \right) \psi_i \right|^2 + \sum_{i}^{N} \alpha_i \left| \psi_i \right|^2 + \sum_{i,j=1}^{N} g_{ij} \left| \psi_i \right|^2 \left| \psi_j \right|^2 \right] \tag{2}$$

is the Hamiltonian. This model is a description of the condensate while the particle content of the system outside the condensate is not captured by equation (2). Here, the field A_μ formally appears as a non-fluctuating gauge-field and parametrizes the angular velocity of the system under rotation. The condensate fields ψ_i are dimensionful complex fields which are allowed to fluctuate both in phase and amplitude. Importantly, the phases are defined with compact support $-\pi < \theta_i \leq \pi$, leading to the appearance of topological defects in the form of vortices (two dimensions) and vortex loops (three dimensions) in the condensate. The model is thus capable of capturing all thermal fluctuations of the condensate, including vortex-fluctuations destroying long-range phase coherence in the condensate. Moreover, i and j are indices running from 1 to N denoting the component of the order parameter (a 'color' index). The parameters α_i and g_{ij} are chemical potentials and interaction parameters of the model, respectively. Φ_0 is the coupling constant to the rotation-induced vector potential, and m_i is the particle mass of species i. For mixtures consisting of different atoms or different isotopes of one atom, the masses will depend on the index i, while for mixtures consisting of same atoms in different hyperfine states, the masses are equal among the components i. The inter- and intra-component coupling parameters g_{ij} are related to real inter- and intra-component scattering lengths a_{ij}, in the following way

$$g_{ii} = \frac{4\pi\hbar^2 a_{ii}}{m_i}, \tag{3}$$

$$g_{ij} = \frac{2\pi\hbar^2 a_{ij}}{m_{ij}}; \ (i \neq j). \tag{4}$$

Here, $m_{ij} = m_i\, m_j/(m_i + m_j)$ is the reduced mass. In this work, we focus on homonuclear condensates with several components in different hyperfine states, i.e. $m_i = m \forall\ i$. Note that when $g_{12} = g_{21} \equiv \lambda g > g_{11} = g_{22} \equiv g$, i.e. $\lambda > 1$, there is a strong tendency in the system to phase separate, leading to two immiscible quantum fluids. For a homonuclear binary mixture, we have $m_{ij} = m_i/2$. Then, it suffices that $a_{ij} > a_{ii}$ for the inter-component density–density interactions to dominate the intra-component density–density interactions.

It is convenient to rewrite the potential (repeated indices are summed over) as follows [27]

$$V \equiv \alpha_i \left| \psi_i \right|^2 + g_{ij} \left| \psi_i \right|^2 \left| \psi_j \right|^2, \tag{5}$$

by introducing interaction parameters η, ω, such that $g = \eta + \omega$, and $\lambda g = \eta - \omega$, i.e. $\eta = g\,(1 + \lambda)/2$, $\omega = g\,(1 - \lambda)/2$. Here, λ denotes the ratio between the inter- and intra-component interactions. Then, equation (5) takes the form (up to an additive constant)

$$V = \left(\alpha_1 + 2\eta\right)\left|\psi_1\right|^2 + \left(\alpha_2 + 2\eta\right)\left|\psi_2\right|^2 + \eta\left(\left|\psi_1\right|^2 + \left|\psi_2\right|^2 - 1\right)^2 + \omega\left(\left|\psi_1\right|^2 - \left|\psi_2\right|^2\right)^2. \tag{6}$$

For $\lambda > 1$, $\omega < 0$, with the proviso that $\eta + \omega = \eta - |\omega| > 0$ for stability. Furthermore, we will assume that $\alpha_1 = \alpha_2$, $\alpha_1 \neq \alpha_2$ acts as an external field conjugate to the pseudo-magnetization of the system.

We discretize the model on a cubic lattice with sides L by defining the order parameter field on a discrete set of coordinates $\psi_i(\mathbf{r}) \rightarrow \psi_{\mathbf{r},i}$, $\mathbf{r} \in (i\hat{\mathbf{x}} + j\hat{\mathbf{y}} + k\hat{\mathbf{z}}|\ i, j, k = 1, \ldots, L)$. The covariant derivative is replaced by a forward difference

$$D_\mu \psi_i(\mathbf{r}) \rightarrow \frac{1}{a}\left(\psi_{\mathbf{r}+a\hat{\boldsymbol{\mu}},i} e^{-iaA_{\mu,\mathbf{r}}} - \psi_{\mathbf{r},i}\right). \tag{7}$$

Here, the lattice version of the non-fluctuating gauge field is parametrized in Landau gauge, $A_{\mu,\mathbf{r}} = (0,\ 2\pi fx,\ 0)$, where f is the number of vortices per plaquette, or filling fraction. The lattice spacing, a, is fixed to be smaller than the characteristic length scale of the variations of the order parameter, and $\hat{\boldsymbol{\mu}} \in (\hat{\mathbf{x}},\ \hat{\mathbf{y}},\ \hat{\mathbf{z}})$ is a unit vector.

Thus, the lattice version of the Hamiltonian we consider is given by

$$\begin{aligned} H = &- \sum_{\substack{\mathbf{r},\hat{\boldsymbol{\mu}} \\ i}} \left|\psi_{\mathbf{r}+\hat{\boldsymbol{\mu}},i}\right|\left|\psi_{\mathbf{r},i}\right| \cos\left(\theta_{\mathbf{r}+\hat{\boldsymbol{\mu}},i} - \theta_{\mathbf{r},i} - A_{\mu,\mathbf{r}}\right) \\ &+ \sum_{\mathbf{r},i}\left(\alpha_i + 2\eta\right)\left|\psi_{\mathbf{r},i}\right|^2 \\ &+ \sum_{\mathbf{r}}\eta\left(\left|\psi_{\mathbf{r},1}\right|^2 + \left|\psi_{\mathbf{r},2}\right|^2 - 1\right)^2 \\ &+ \sum_{\mathbf{r}}\omega\left(\left|\psi_{\mathbf{r},1}\right|^2 - \left|\psi_{\mathbf{r},2}\right|^2\right)^2. \end{aligned} \tag{8}$$

Here, we have written the order parameter fields as real amplitudes and phases, $\psi_{\mathbf{r},i} = |\psi_{\mathbf{r},i}|\ e^{i\theta_{\mathbf{r},i}}$. In addition, we have defined an energy scale, $J_0 = \alpha_0^2 a^3/g_0^3$, where α_0 and g_0 are the parameters of the GL theory at $T = 0$. Throughout, we fix $\eta = 5.0$ and $\alpha_1 + 2\eta = \alpha_2 + 2\eta = 0$. This guarantees a non-zero ground state condensate density for all values of ω.

2.2. Ground state symmetry

Equation (8) defines two superfluids coupled by density–density interactions. When there is no phase separation, we have a U(1) × U(1) symmetry broken in the ground state. When the inter-component interaction is equal to the intra-component interaction the system breaks $SU(2)$ symmetry. Here, we are interested in the phase separated case. In this case, the system breaks an additional $\mathbb{Z}_2$ symmetry, corresponding to interchanging $\psi_1 \leftrightarrow \psi_2$. That is, when $\omega > 0$, $|\psi_1|^2 = |\psi_2|^2$ is favored. This represents a $\mathbb{Z}_2$ -symmetric state. On the other hand, when $\omega < 0$, $|\psi_1|^2 \neq |\psi_2|^2$ is favored, such that $|\psi_1|^2 - |\psi_2|^2$ may acquire a nonzero expectation value, with equal probabilities that the expectation value is either positive or negative. This corresponds to breaking an Ising-like $\mathbb{Z}_2$ symmetry. Thus, the ground state breaks a composite $U(1) \times Z_2$ symmetry.

2.3. Observables

The equilibrium phases of the model are characterized by several order parameters. To identify the Ising-like, phase separated order of the system we define

$$\Delta = \left|\left\langle\left|\psi_1\right|^2\right\rangle - \left\langle\left|\psi_2\right|^2\right\rangle\right|, \tag{9}$$

where $\langle|\psi_i|^2\rangle$ is the thermal and spatial average of $|\psi_i(\mathbf{r})|^2$

$$\left\langle\left|\psi_i\right|^2\right\rangle = \left\langle\frac{1}{L^3}\sum_{\mathbf{r}}\left|\psi_{i,\mathbf{r}}\right|^2\right\rangle. \tag{10}$$

A finite value of Δ signals relative density depletion in either of the condensates. In addition to $\mathbb{Z}_2$ order, it is important to monitor the U(1) ordering of the system. The helicity modulus measures phase coherence along a given direction of the system. It is defined as

$$\Upsilon_{\mu,i} = \frac{1}{L^3}\frac{\partial^2 F\left[\theta'\right]}{\partial\delta_\mu^2}\bigg|_{\delta_\mu=0}. \tag{11}$$

Here, $F[\theta']$ is the free energy with an infinitesimal phase twist, δ_μ, applied along the μ-direction, *i.e.*, we make the replacement

$$\theta_{\mathbf{r},i} \rightarrow \theta'_{\mathbf{r},i} = \theta_{\mathbf{r},i} - \boldsymbol{\delta} \cdot \mathbf{r} \tag{12}$$

in F.

We also identify the nature of the phases by computing thermal averages of real-space configurations of densities $\langle |\psi_i(\mathbf{r}_\perp)|^2 \rangle$ and vortices $\langle |n_i(\mathbf{r}_\perp)|^2 \rangle$ in the system. These are computed by averaging the quantity along the z-direction of the system, with subsequent thermal averaging. That is

$$\left\langle n_i\left(\mathbf{r}_\perp\right)\right\rangle = \left\langle \frac{1}{L_z}\sum_z n_{i,\mathbf{r}} \right\rangle. \tag{13}$$

and

$$\left\langle \left|\psi_i\left(\mathbf{r}_\perp\right)\right|^2 \right\rangle = \left\langle \frac{1}{L_z}\sum_z \left|\psi_{i,\mathbf{r}}\right|^2 \right\rangle. \tag{14}$$

The vorticity, $n_{i,\mathbf{r}}$ is calculated by traversing a plaquette with surface normal in the z-direction, adding the phase difference $\theta_{\mathbf{r}+\hat{\boldsymbol{\mu}},i} - \theta_{\mathbf{r},i} - A_{\mu,\mathbf{r}}$ on each link. If this plaquette sum turns out to have a value outside the primary interval, $(-\pi, \pi]$, $2n\pi$ $(-2n\pi)$ is added to the sum, which inserts a vortex of charge $+n$ $(-n)$ on the plaquette.

To further characterize vortex structures, we examine the structure factor of the vortices, defined as

$$S_i\left(\mathbf{q}_\perp\right) = \left\langle \left| \frac{1}{L^3 f}\sum_{\mathbf{r}_\perp, z} n_{i,\mathbf{r}} e^{\mathrm{i}\mathbf{q}_\perp \cdot \mathbf{r}_\perp} \right|^2 \right\rangle. \tag{15}$$

This is simply the Fourier-transform of the z-averaged vorticity. To improve the resolution of the interesting q-vectors, we remove the $\mathbf{q}_\perp = 0$ point from the figures. We also calculate

$$\max\left(S_i\left(\mathbf{q}_\perp\right)\right) = \left\langle \max\left(\left| \frac{1}{L^3 f}\sum_{\mathbf{r}_\perp, z} n_{i,\mathbf{r}} e^{i\mathbf{q}_\perp \cdot \mathbf{r}_\perp} \right|^2 \right) \right\rangle, \tag{16}$$

in order to monitor the development of peaks in the structure factor across transition points.

We also compute the specific heat capacity

$$\frac{C_V L^3}{\beta^2} = \langle (H - \langle H \rangle)^2 \rangle. \tag{17}$$

as a means of precisely locating the various transition points.

2.4. Details of the Monte-Carlo simulations

We consider the model on a lattice of size $L_x \times L_y \times L_z$, using the Monte-Carlo algorithm, with a simple restricted update scheme of each physical variable, and Metropolis–Hastings [28, 29] tests for acceptance. Here, L_i is the linear extent of the system in the Cartesian direction $i \in (x, y, z)$. In all our simulation, we have used cubic systems $L_x = L_y = L_z = L$, with $L \in \{32, 64, 96\}$. At each inverse temperature, 10^6 Monte-Carlo steps are typically used, while 10^5 additional sweeps are used for equilibration. Each Monte-Carlo step consists of an attempt to update each amplitude and phase separately in succession, at each lattice site. To improve acceptance rates, we only allow each update to change a variable within a limited interval around the previous value, the size of which is chosen by approximately maximizing acceptance rates and minimizing autocorrelations. The Mersenne–Twister algorithm is used to generate the pseudo-random numbers needed [30]. To ensure that the state is properly equilibrated, time series of the internal energy measured during equilibration are examined for convergence. To avoid metastable states, we make sure that several simulations with identical parameters and different initial seeds of the random number generator anneals to the same state. Measurements are post-processed with multiple histogram reweighting [31]. Error estimates are determined by the jackknife method [32].

3. Mixing and superfluid phase transitions in the presence of rotation

In this section we consider the effect of imposing a finite rotation on the condensate. Our main results are presented for a system size of $L = 64$ and $f = 1/32$, but we have considered system sizes $L \in \{32, 64, 96\}$.

Introducing a finite amount of (rotation-induced) vortices in the ground state significantly alters the simple arguments regarding the expected ground state symmetry presented above. The effect of the vortices is to suppress the parameter regime where a broken $\mathbb{Z}_2$ symmetry is found, $\Delta \neq 0$. Recall that for $f = 0$, the ground state the broken $\mathbb{Z}_2$ symmetry will reduce the condensate to a single component condensate with a single broken U(1) symmetry in the ground state. A finite amount of vortices alters this. Vortices interact via long range current–current interactions. It is energetically favorable to maximize the distance between vortices, subject to

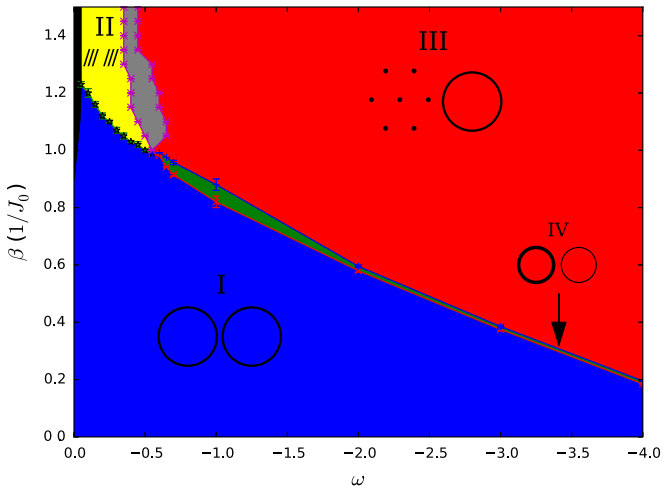

Figure 1. The phase diagram of the two-component Bose–Einstein condensate at finite rotation, $f \neq 0$, $\eta = 5$, and $\omega < 0$. Negative ω may lead to the breaking of the $\mathbb{Z}_2$ -symmetry in the problem, in addition to the usual breaking of the obvious $\mathrm{U}(1) \times \mathrm{U}(1)$ -symmetry. Region I is a $\mathbb{Z}_2$ - as well as $\mathrm{U}(1) \times \mathrm{U}(1)$ -symmetric two-component vortex-liquid phase. Region II is a $\mathbb{Z}_2$ -symmetric striped (nematic) phase consisting of a two-component vortex liquid with broken translational symmetry in a direction perpendicular to the stripes, but not in the direction parallel to the stripes. Region III is a phase with broken $\mathbb{Z}_2$ -symmetry, and with broken translational symmetry in one condensate component, but not the other. Region IV is similar to Region III, except that no translational symmetry is broken in either condensate component. The gray region represents upper and lower bounds of the transition line between Region II and III. Details are explained in the main body of the paper.

the constraint that a specific number of them has to be contained within a given area perpendicular to the direction of rotation. This effect leads to a uniform distribution of minima (equivalently maxima) in the condensate densities. On the other hand, density suppression by vortices in one component in general allows the densities in the second component to nucleate. The short-range repulsive inter-component density–density interaction $(\eta - \omega)(|\psi_1|^2|\psi_2|^2 + |\psi_2|^2|\psi_1|^2)$ (which exceeds the intra-component density–density interaction $(\eta + \omega)(|\psi_1|^2|\psi_1|^2 + |\psi_2|^2|\psi_2|^2)$ for $\omega < 0$), tends to produce regions where the density one component is large while the other is small, and vice versa. Below a critical value of $-\omega = -\omega_c \approx +0.6$, we do not see any onset of $\Delta \neq 0$ at any value of β as the system is cooled from a uniform state. That is, the interface tension between the phases is sufficiently low and the overall free energy, which includes long range inter vortex interaction, is minimized by the state with $\Delta = 0$.

For the subsequent discussion, it helps to consider a schematic phase diagram of the system with $f \neq 0$, which we have obtained through large-scale Monte-Carlo simulations. The phase diagram is shown in figure 1. Region I denotes the simple translationally invariant high-temperature $\mathbb{Z}_2$ - and $\mathrm{U}(1) \times \mathrm{U}(1)$ -symmetric two-component phase with equal densities of both condensate components. Region II shows the $\mathbb{Z}_2$ -symmetric striped phase. Region III is a region with broken $\mathbb{Z}_2$ -symmetry, with one high-density condensate component in a uniform hexagonal vortex lattice phase, and one low-density component in a uniform vortex liquid phase. The gray region separating Region II and III represents upper and lower bounds of the transition between Region II and III. Region IV is a region with broken $\mathbb{Z}_2$ -symmetry, but with the two condensates both in a vortex-liquid phase. Thus, the phase transition separating Region I from Region II is a phase-transition line separating a two-component isotropic vortex liquid from a two-component striped (nematic) vortex liquid. The line separating Region I from Region IV is one where a $\mathbb{Z}_2$ -symmetry is broken, and the line separating Region II from Region IV is one where a translational symmetry is broken and the system acquires non-zero helicity modulus

3.1. Transition from Region I to Region II

We first consider the thermally driven transition from the high-temperature symmetric two-component vortex liquid phase, Region I, to the low-temperature two-component striped (nematic) phase, Region II, for fixed negative ω, but where $|\omega| < |\omega_c|$, i.e. to the left of the splitting point where Region IV opens up.

In figure 2 we show the specific heat c_V, helicity moduli in the z-direction $\Upsilon_{z,i}$ as the inverse temperature β is varied, for $f = 1/32$ and $\omega = -0.50$. This corresponds to a value of $-\omega$ to the left of the splitting point where Region IV opens up (see figure 1). The longitudinal helicity moduli $\Upsilon_{z,i}$ of both components develop a finite expectation value. The onset of this finite value is accompanied by an anomaly in the specific heat.

We note the sharp, δ-function anomaly in the specific heat and the discontinuous behavior of the helicity moduli in both components. These features are all straightforwardly interpreted as signals of a first-order phase transition. This is furthermore borne out by performing a computation of the histogram of the free energy

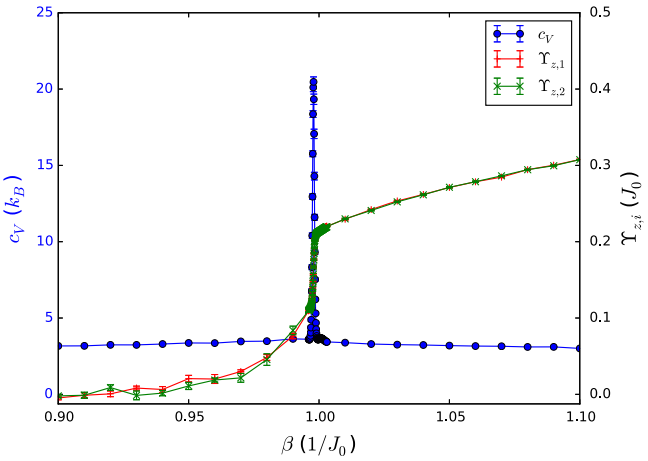

Figure 2. Specific heat, c_V, and helicity moduli along the z-axis , $\Upsilon_{z,i}$, with $f = 1/32$ and $\omega = -0.50$, i.e as the system transitions from Region I to Region II in figure 1.

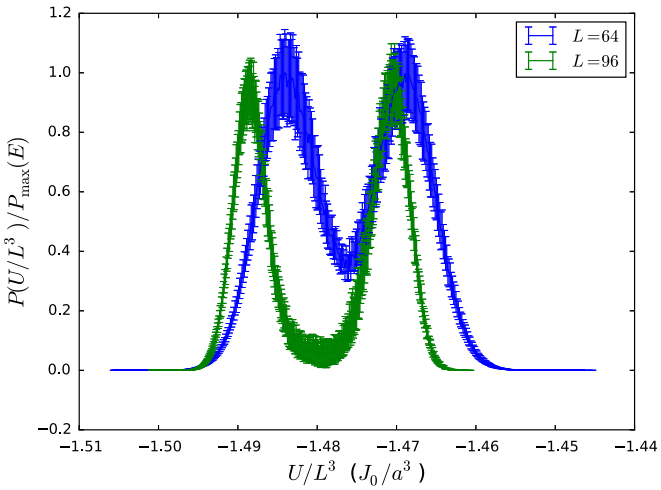

Figure 3. Histograms of the probability distribution of the internal energy per site, U/L^3, at the transition point $\omega = -0.5$, $\beta \approx 0.9995$, separating Region I from Region II in figure 1, for $L = \{64,\ 96\}$. Multi-histogram reweighting was used to obtain histograms with approximately equal peak heights.

versus internal energy of the system at precisely at the transition, see figure 3. This shows a double-dip structure with a peak in between, the standard hallmark of two degenerate coexisting states separated by a surface whose energy is given by the height of the peak between the minima. This surface energy clearly scales up with system size (more precisely it scales with the cross-sectional area of the system), while the difference between the energies separating the two degenerate states approaches a finite value as the system size increases. The histograms develop into two separate δ-function peaks as the system size increases, while the difference in the internal energy between the two degenerate states of equal probability (equivalently of equal free energy) is the latent heat of the system. The latter clearly approaches a finite value per degree of freedom as the system size increases, demonstrating the first-order character of the transition.

To further characterize the transition I $\rightarrow$ II, figure 4, shows the $\mathbb{Z}_2$ order parameter Δ and the structure functions $S_i(\mathbf{q}_\perp)$, $i \in (1,\ 2)$ in a narrow range around the transition point. From the top panel, it is seen that $\Delta = 0$ for all β considered. Moreover, we see that as β is increased, the maximum value of the structure function, corresponding to the developing Bragg peaks in the low temperature phase are significantly increased at the transition temperature. The maximum is measured by averaging the maximum of the structure function at each measurement, regardless of location, hence the actual value may differ from what is seen in the bottom panel of figure 4. The onset of the latter marks the transition from a uniform two-component vortex liquid to a two-component nematic vortex liquid, a striped phase. The mechanism for producing the striped phase is described above. In the striped phase, it is difficult to equilibrate the system at each new temperature step with only local MC-updates, as is evident from the noise in the structure functions seen on the low temperature side

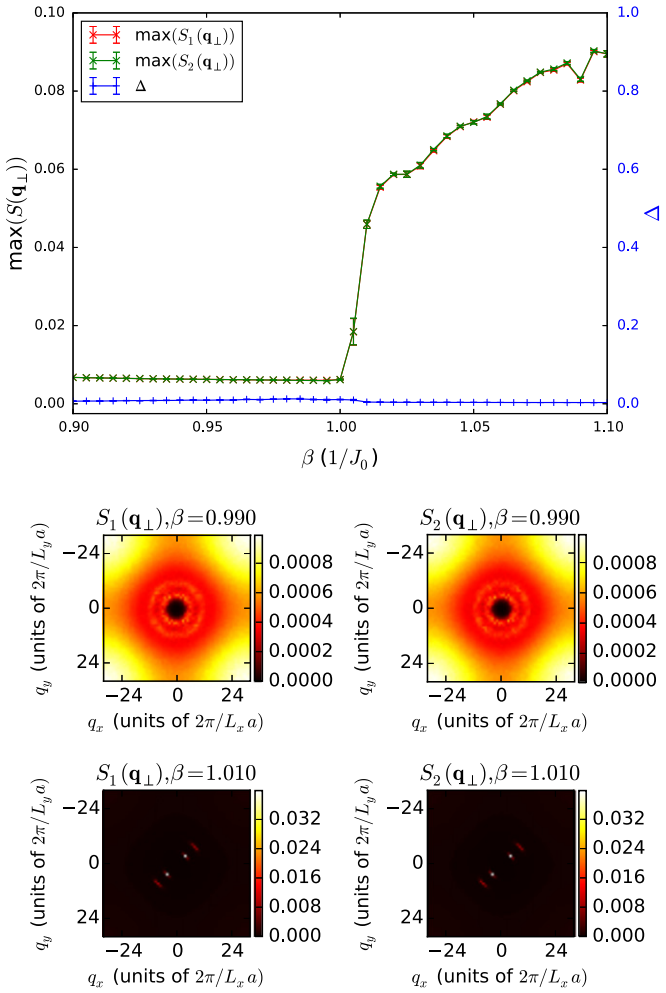

Figure 4. $\mathbb{Z}_2$ order parameter Δ and vortex structure functions $S_i(\mathbf{q}_\perp)$, $i \in (1, 2)$ in the vicinity of the transition from Region I to Region II, figure 1, with $f = 1/32$, $\omega = -0.50$. The top panel shows Δ as a function of β, as well as maxima of the structure functions $\max\left(S_i(\mathbf{q}_\perp)\right)$. The four bottom panels show the structure functions $S_1(\mathbf{q}_\perp)$ and $S_2(\mathbf{q}_\perp)$ for the two values $\beta = 0.990$ and $\beta = 1.010$.

of the top panel of figure 4. This noise would most likely be improved by using different approaches, for instance cluster algorithms. However, the noise does not alter our conclusions regarding the transition, or the nature of the striped phase. Note that in the thermodynamic limit, isolated vortex sheets can be expected to be in the state of one-dimensional (1D) liquid at any finite temperature in analogy with the absence of crystalline order in 1D systems.

We thus conclude that the transition from Region I to Region II is a first order phase-transition involving the breaking of a composite $\mathrm{U}(1) \times \mathrm{U}(1)$ symmetry, from an isotropic two-component vortex liquid in Region I to a two-component nematic phase of intercalated lattices of stripes of 1D vortex liquids in Region II. We next go on to consider in some more detail the structure functions, primarily to gain more insight into the character of the striped phase of Region II.

The four bottom panels of figure 4 show the structure functions $S_i(\mathbf{q}_\perp)$, $i \in (1, 2)$ at two values of β, $\beta = 0.990$ and $\beta = 1.010$. At $\beta = 0.990$, both structure functions show ring-like structures characteristic of an isotropic liquid. Notice also that the intensity of the rings are equal, which is a consequence of the fact that $\Delta = 0$. At $\beta = 1.010$, both structure functions have developed Bragg peaks in one direction bot no Bragg peaks in the corresponding perpendicular direction. This is indicative of a striped phase.

This may be further corroborated by correlating the structure functions with real-space vortex structures for various values of β. This is shown in figure 5.

One aspect of the structure functions shown in the two bottom rows of figure 5, is particularly important. Consider first the case $\beta = 0.900$, well within Region 1 for $\omega < \omega_c$. This is shown in the leftmost column of figure 5. The real-space vortex configurations in both components are disordered. Moreover, $S_i(\mathbf{q}_\perp)$, $i \in (1, 2)$ both components feature ring-structures characteristic of an isotropic liquid phase. The value of $|\mathbf{q}|$ at which the rings appear is a measure of the average inverse separation between the vortices in the isotropic liquids. The intensities of both structure functions is the same. Consider next the case $\beta = 0.995$, shown in the middle

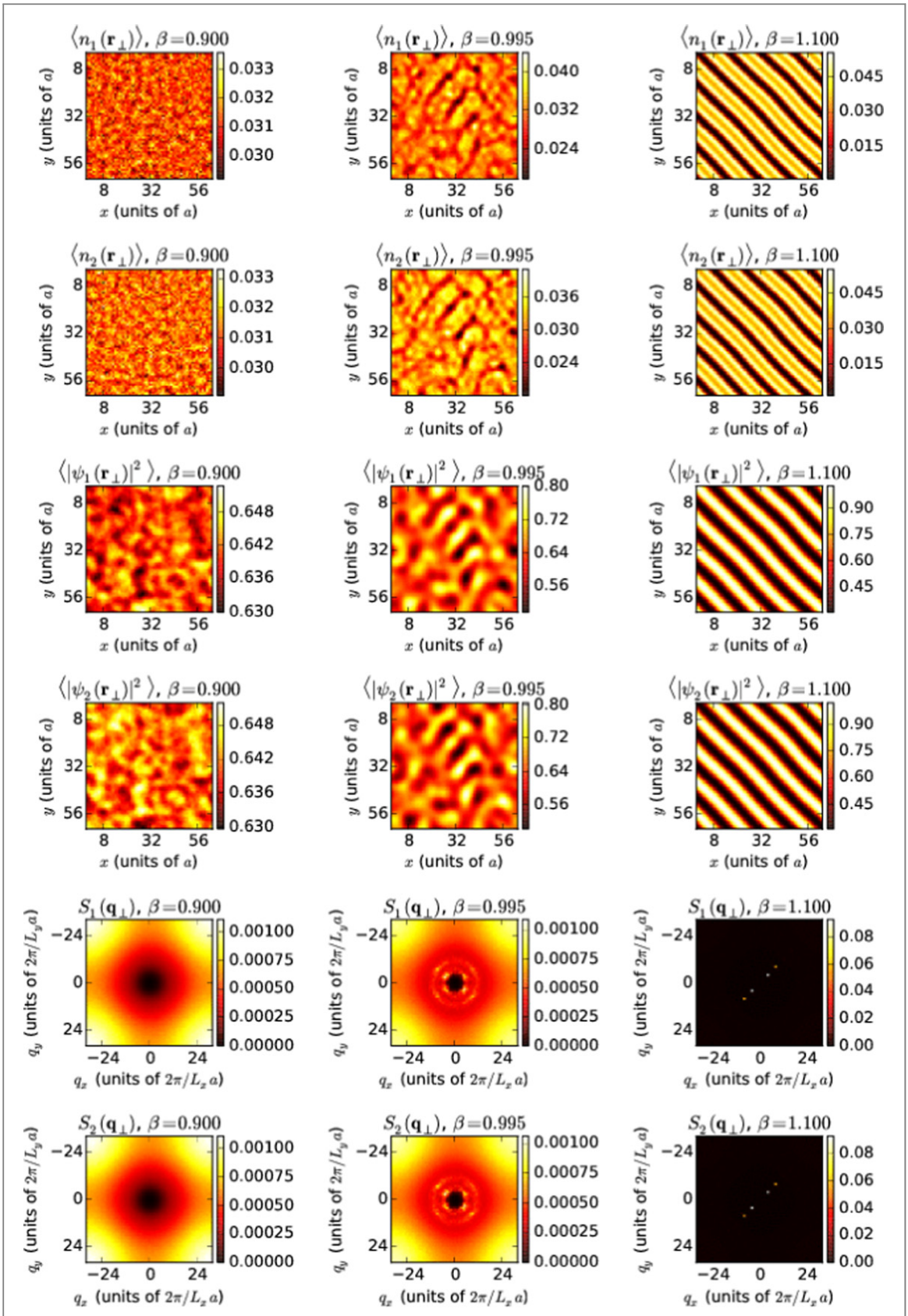

Figure 5. Tableaux showing detailed real space and reciprocal space pictures of the transition from Region I to Region II. The inverse temperature is varied between each column, $\beta \in \{0.900,\ 0.995,\ 1.100\}$. Each row shows averaged vortex densities of each component, $\langle n_i(\mathbf{r}_\perp)\rangle$, averaged amplitude densities of each component, $\langle|\psi_i(\mathbf{r}_\perp)|\rangle$, and vortex structure functions of each component, $S_i(\mathbf{q}_\perp)$. The leftmost column corresponds to an inverse temperature well within Region I, the middle column is at an inverse temperature just below the transition into Region II, while the rightmost column is well within Region II.

column of figure 5. From the real-space pictures, one discerns a tendency towards stripe-formation. This is reflected in $S_i(\mathbf{q}_\perp)$, $i \in (1, 2)$, where the ring-like structures now instead are anisotropic, developing peaks in the direction perpendicular to the direction of the incipient stripes. At even lower temperatures $\beta = 1.100$, well within Region II where stripes are fully developed, the tendency towards anisotropies in $S_i(\mathbf{q}_\perp)$, $i \in (1, 2)$ is even more obvious. This is shown in the rightmost column of figure 5. In this case, Bragg-peaks have fully developed in the directions perpendicular to the stripes. There are, however, no Bragg peaks in the direction parallel to the stripes. If the stripes were perfectly straight, there would be two weak Bragg peaks in these directions. This would be the 1D analog of the ring-like liquid structures of the isotropic liquid. The value of $|\mathbf{q}|$ at which this single weak peak occurs corresponds to the inverse average separation between vortices within the stripes. The reason they are not observed in our calculations, is due to the slight fluctuations in the shape of the stripes, which wash the Bragg peaks out.

We thus conclude that Region II is a striped phase where the stripes form 1D vortex liquids. Vortices in quasi-1D systems have finite energy and cannot form a 1D solid at any finite temperature. This is consistent with the structure factor we observe. On the other hand, the interaction between stripes may not be negligible, so the details of the phase diagram in Region II warrant further investigation. A notable feature of this state is the finite helicity modulus in z-direction, even if the structure factors show absence of vortex ordering within stripes. This highly unusual situation originates with the positive interface energy between the two condensates. That is, consider a stripe-liquid in x-direction. A vortex line in the z-direction is free to execute transverse meanderings in the x-direction. A superflow in the z-direction would produce a y-component of the Magnus-force on the x-components of the fluctuating vortex lines. However, vortex segments are restrained from moving in y-direction due to the stripe interface tension. This results in the observed finite helicity modulus in z-direction. Similar results are found for a number of other ω-values we have considered, for[4] $-\omega < 0.6$.

3.2. Transition from Region I to Region III, via Region IV

Increasing $-\omega$ further, such that the inter-species density–density interaction increases, eventually favors a different pattern of phase-separation of the two components, despite the effect of long-range current–current interactions between rotation-induced vortices promoting uniform density distributions. This leads to a broken $\mathbb{Z}_2$ -symmetry. The condensate component with a globally suppressed density will therefore be in a vortex-liquid phase while the condensate component with globally enhanced density will be in a vortex lattice phase. Thus, the broken symmetries of the ordered phase are $\mathrm{U}(1) \times \mathbb{Z}_2$, and the breaking of these symmetries are split into two separate transitions. The splitting occurs because the $\mathrm{U}(1)$ -sector directly couples to the rotation, while the $\mathbb{Z}_2$ -sector does not. The phase-transition in the stiff $\mathrm{U}(1)$ -sector, which is a vortex-lattice melting, is therefore separated from the $\mathbb{Z}_2$ -transition by an amount which depends on f.

This is illustrated in figure 6, showing Δ, specific heat C_V, and $\Upsilon_{z,1}$, $\Upsilon_{z,2}$ as functions of β. The $\mathbb{Z}_2$ order parameter Δ has an onset at $\beta_{\mathbb{Z}_2}$, at which the specific heat has an anomaly. This transition is a transition where an Ising like order parameter is broken, and can be continuous. There is no onset of $\Upsilon_{z,2}$, showing that component 2 remains in a vortex liquid phase. Component 1 forms a vortex solid at lower temperature, as evidenced by the onset of $\Upsilon_{z,1}$. This happens at a $\beta_{\mathrm{U}(1)}$ which is separated from $\beta_{\mathbb{Z}_2}$, as explained above. The freezing of component one is effectively a freezing transition of a single component, and is therefore expected to be a first-order transition. Accompanying this one would expect to see a second, smaller anomaly in the specific heat, at a lower temperature. This is not observed in the simulations performed, as the small anomaly is completely overshadowed by the large specific heat peak from the $\mathbb{Z}_2$ transition.

Figure 7 shows the structure functions $S_1(\mathbf{q}_\perp)$ and $S_2(\mathbf{q}_\perp)$ at $\omega = -4.0$ at three different values of β, namely $\beta = (0.184,\ 0.190,\ 0.195)$. These values correspond to Regions I, IV, and III in figure 1, respectively. Here again, we see the freezing of one component across the transition, while the other component remains in the liquid phase. The additional information we get out of these panels is that one component remains an *isotropic* vortex liquid, while the other component freezes into a hexagonal vortex liquid. This sets the low-temperature Region III (see figure 1) at $\omega = -4.0$ drastically apart from the low-temperature Region II (see figure 1) at $\omega = -0.50$. The latter features a low-temperature two-component nematic vortex liquid phase with broken rotational invariance, the former case features a low-temperature mixed isotropic vortex liquid/hexagonal vortex lattice phase.

Taking figure 1 and figure 6 at face value, suggests that two separate transitions exist. However, one cannot entirely rule out finite-size artifacts associated with a single transition where the onset of $\Upsilon_{z,1}$ would coincide with the onset of Δ in figure 6. By examining the structure factors, examples of which are shown in the middle panel of figure 7 it is evident that a relatively large intermediate regime corresponding to Region IV is observed. From the sharp onset of Δ, accompanied by the specific heat peak, we determine the transition temperature for

[4] We also observed much smaller but finite helicity modulus in the direction perpendicular to stripes, which we interpret as a consequence of weak standard geometric pinning of domain walls.

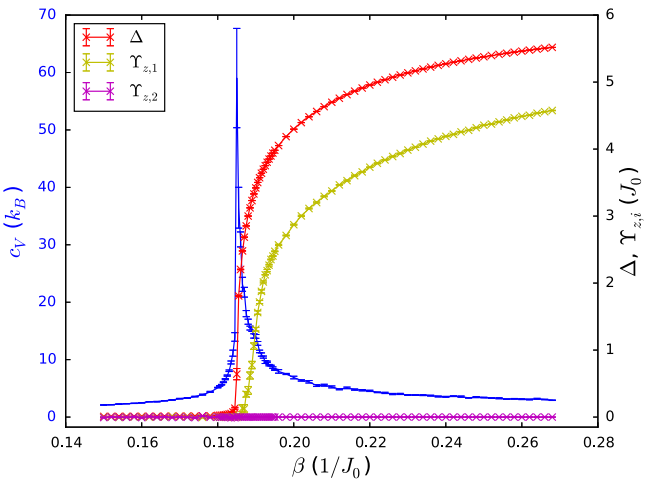

Figure 6. The phase transitions between Region I and Region IV, and between Region IV and Region III, for $f = 1/32$, $\omega = -4.0$, and $L = 64$. Note the separation between the onset of Δ and $\Upsilon_{z,i}$. The onset of Δ signals the breaking of a $\mathbb{Z}_2$ -symmetry, along with the associated anomaly in specific heat C_V. This marks the transition from Region I to Region IV in figure 1. In Region IV, we have $\Delta \neq 0$, while both components remain in isotropic vortex liquid states. In passing from Region IV to Region III in figure 1, the onset of one of the helicity moduli, $\Upsilon_{z,1}$ say, signals the freezing of the vortex liquid in the corresponding component, while the absence of an onset of the helicity modulus, $\Upsilon_{z,2}$ say, in the other component shows that this component remains in a vortex liquid phase. The onset of $\Upsilon_{z,1}$ signals the breaking of a U(1) -symmetry associated with vortex-liquid freezing.

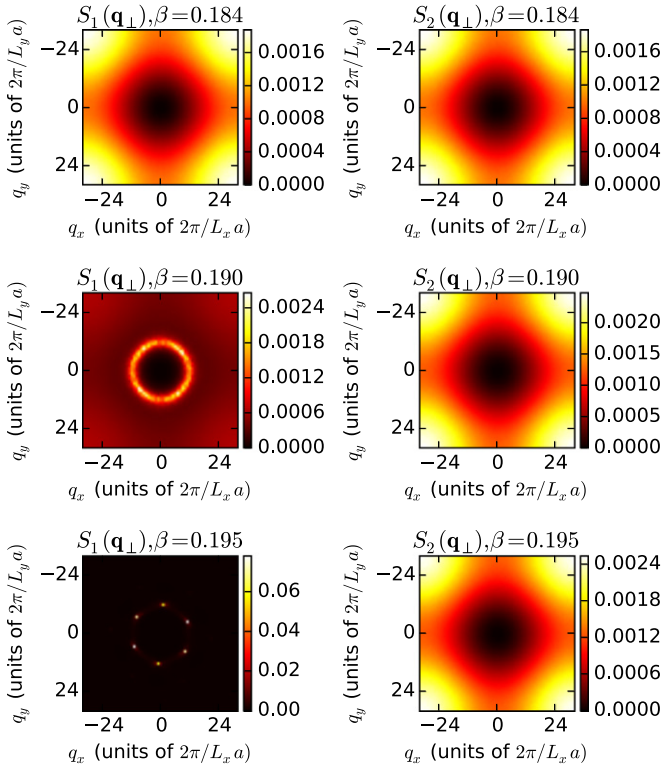

Figure 7. The phase transitions of the system for $f = 1/32$, $\omega = -4.0$. Structure functions $S_1(\mathbf{q}_\perp)$ and $S_2(\mathbf{q}_\perp)$ at three different values of β, namely $\beta = (0.184,\ 0.190,\ 0.195)$, corresponding to Regions I, IV, and III in figure 1, respectively.

the $\mathbb{Z}_2$ symmetry breaking to be $\beta_{\mathbb{Z}_2} = 0.1850(5)$. The appearance of six sharply defined Bragg peaks in the structure factor, appear at a lower temperature $\beta = 0.195(1)$. The onset of $\Upsilon_{z,1}$ prior to the appearence of the Bragg peaks may be a finite size effect. That being said, simulating larger system sizes may also alter the details of the transition temperatures.

On general grounds one may expect that phase IV should exist. The simulations unambiguously identify a state where one component has a vortex lattice while the other component with a suppressed density is in a state of tensionless vortex matter. Since a vortex liquid can form due to positional disorder of tension-full vortex lines,

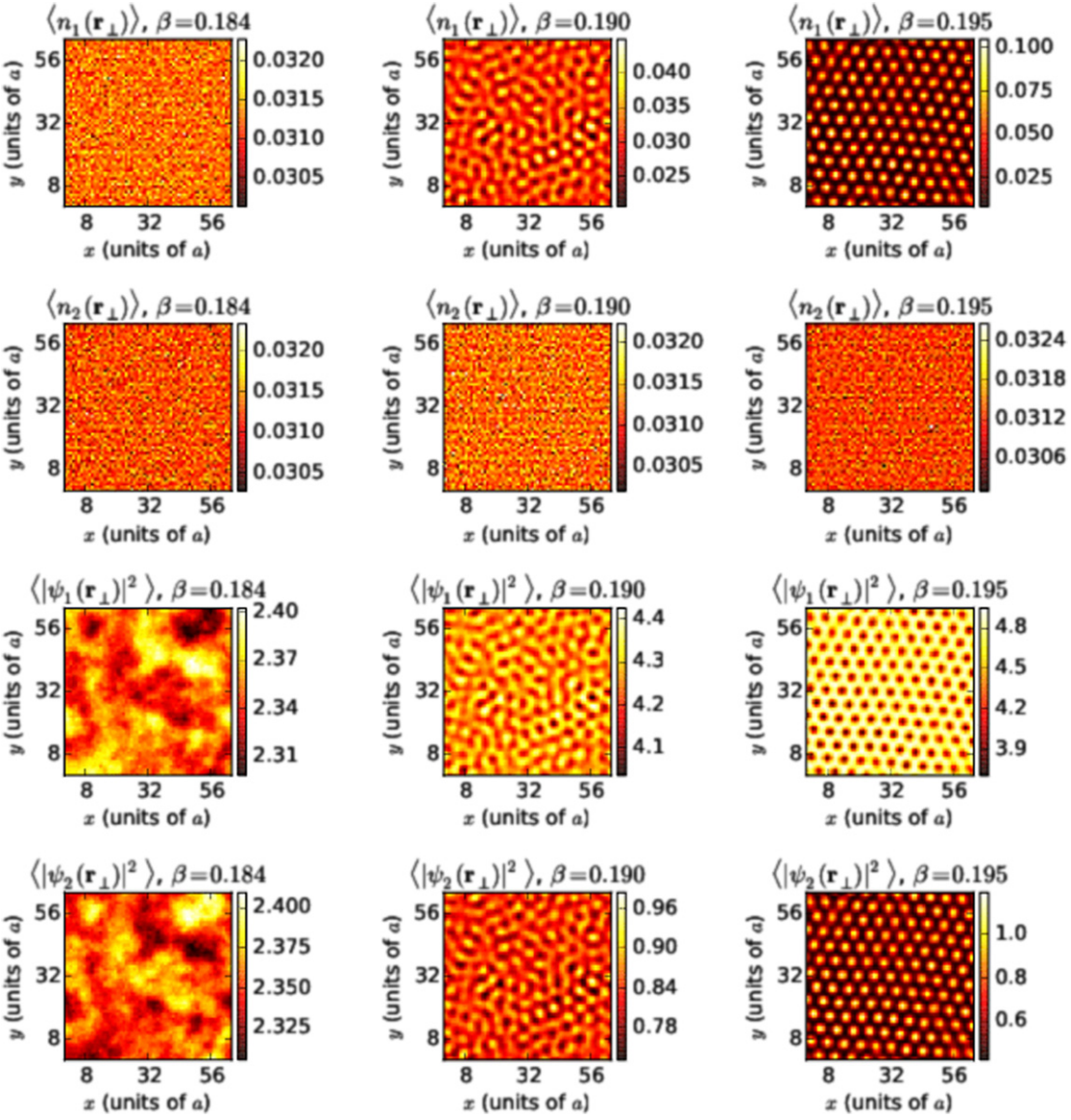

Figure 8. Tableaux showing detailed real space pictures of the transition from Region I to Region III, via Region IV. The inverse temperature is varied between each column, $\beta \in \{0.184,\ 0.190,\ 0.195\}$, and $\omega = -4$. Each row shows, from top to bottom, averaged vortex densities of each component, $\langle n_i(\mathbf{r}_\perp)\rangle$, and averaged amplitude densities of each component, $\langle|\psi_i(\mathbf{r}_\perp)|\rangle$. Note the vortex-ordering in one of the components, and the lack of vortex-ordering in the other component, as the system transitions from the symmetric phase Region I ($\beta = 0.184$) to the low-temperature phase Region III ($\beta = 0.195$). Note also the disparity in density-amplitudes in the two components in the intermediate regime Region IV ($\beta = 0.190$), due to the $\mathbb{Z}_2$ -symmetry breaking.

it can be expected that the tension-full vortex liquid in the dominant component still suppresses the density of subdominant component leading to the appearance of the state IV. Alternatively, suppose that one starts out from a low-temperature phase-separated state where one components is in a vortex lattice state and the other component effectively has a much lower density. The vortex lattice of the dominant component may melt without affecting the density in this component, since vortex-lattice melting is driven by phase-fluctuations of the superfluid order parameter, not density fluctuations. Further investigation of this part of the phase diagram is warranted.

For a more detailed overview of the transition, figure 8 shows the evolution of $\langle n_i(\mathbf{r}_\perp)\rangle$, $\langle|\psi_i(\mathbf{r}_\perp)|\rangle$, and $S_i(\mathbf{q}_\perp)$ across the three Regions, I, IV, and III. If one follows the evolution of the vortex densities in each component, it is seen that the component which acquires a low stiffness in Region IV and III is virtually unchanged, i.e. it remains in a completely uniform state. The other component, on the other hand, evolves from a uniform state in Region I, through being close to freezing into a hexagonal lattice in Region IV, and finally into a hexagonal structure in Region III. The amplitude densities corroborate this picture. In Region I they are on average equal and uniform, while in Region IV the difference in stiffness is clearly seen. Here some inhomogeneities arise in the stiff component as the vortices are close to entering a hexagonal phase, which is also reflected in the soft component simply because of the local intercomponent repulsion. In Region III, the

amplitude density of the stiff component is high and uniform with small dips corresponding to each vortex. The soft component is low and uniform with small peaks, again due to intercomponent interactions.

3.3. Transition from Region II to Region III

Finally, we consider the transition from Region II to Region III. In Region II, we have $\Delta = 0$, while in Region III, $\Delta \neq 0$. Therefore the Regions II and III are separated by a $\mathbb{Z}_2$ -symmetry breaking. Stripe-forming systems in general have complicated structural transitions. We find an intermediate regime where the lattice of stripes has disordered, but where the hexagonal lattice/isotropic liquid-mixture has not yet fully developed. This results in multiple metastable, but robust coexisting phases of vortices in components 1 and 2 residing in different parts of the condensate. These two coexisting phases are separated by a surface of positive surface energy. This surface constrains the motion of vortex systems. As a result, in the finite systems which we simulate, the helicity modulus $\Upsilon_{z,i}$ acquire nonzero values in both components in this intermediate regime.

As $-\omega$ is increased further, such that one component becomes dominant and the other is suppressed, the minor component becomes normal. Note that when the inclusions of the normal component become isolated, they represent quasi-1D subsystems. Quasi-1D systems are superfluid only at zero temperature. However, simulations on finite systems may still display finite helicity modulus. As the density of the component increases, the corresponding intra-component current–current interaction between the rotation-induced vortices in this component increases. Hence, the intra-component long-range interaction for this component dominates, and a hexagonal vortex-lattice results. Consequently, the helicity-moduli in the two components have quite different behavior as $-\omega$ increases. In the component that eventually takes up a vortex lattice state, it increases monotonically with $-\omega$. In the other component, it is non-monotonic as a function of ω, eventually approaching 0 deep into Region III.

Typical examples of the vortex structures that appear between Region II and Region III in figure 1 are shown in figure 9. These are all metastable, long-lived states which prevent equilibration of the system. We have been unable to locate the sharp separatrix between these two regions, and whether there are other stable intermediate phases due to the lack of equilibration. Note that this problem is known in other stripe-forming systems where phases are separated by metastable and glassy states [41, 42]. The gray area in figure 1 represents upper and lower bounds for the transition. The bounds were determined by determining the parameter range where the simulation equilibrates to either striped or hexagonal/liquid separated configurations, exclusively.

4. Conclusions

In this paper, we have considered the states of a two-component BEC in the situation where inter-component density–density interactions dominate the intra-component density–density interactions. The two components of the condensate are assumed to be comprised of homonuclear atoms in two different hyperfine states. The problem features an Ising-like symmetry. This Ising (or $\mathbb{Z}_2$) symmetry emerges from the dominance of the inter-component interactions over the intra-component ones. The spontaneous breaking of this Ising-symmetry corresponds to a spontaneously generated, interaction-driven, imbalance between condensates in different hyperfine states.

At finite rotation, we find four regions, denoted Regions I, II, III, and IV, of thermodynamically stable states, see figure 1. Region I is a high-temperature regime where the system remains in a two-component isotropic vortex liquid phase with equal densities of both components. Region II is a nematic phase (broken rotational symmetry) with ordered stripes of 1D vortex liquids, and with equal densities in different components. This state features a spontaneously broken composite $\mathrm{U}(1) \times \mathrm{U}(1)$ -symmetry, but is $\mathbb{Z}_2$ -symmetric. In addition it spontaneously breaks translation symmetry in one direction due to formation of periodic modulation of condensate densities. Region III is a mixed state with one component in a $\mathrm{U}(1)$ -symmetric isotropic vortex liquid phase while the other component resides in a hexagonal vortex lattice phase with broken $\mathrm{U}(1)$ -symmetry. The origin of the different behaviors of the two components is that Region III also features a spontaneously broken $\mathbb{Z}_2$ -symmetry, i.e. a difference in the densities of the two components. The component with a large density has higher phase stiffness than the component with the lower density, hence the discrepancy in their vortex states. Finally, Region IV is a region intermediate between Region I and Region III, in which $\mathrm{U}(1)$ -symmetry is not broken in either of the components, but where a spontaneously generated imbalance between densities of hyperfine states exists. Both components are in an isotropic and disordered vortex state.

The phase transition from Region I to Region II in figure 1 is a first-order composite $\mathrm{U}(1) \times \mathrm{U}(1)$ transition. The phase transition between Region I and Region IV is associated with a spontaneous $\mathbb{Z}_2$ symmetry breaking where a difference in densities of the two condensates sets in. The phase-transition between Region IV and Region III is a first order $\mathrm{U}(1)$ transition associated with the freezing of an isotropic vortex liquid in one component into a hexagonal vortex lattice in the same component, while the other component (the one with

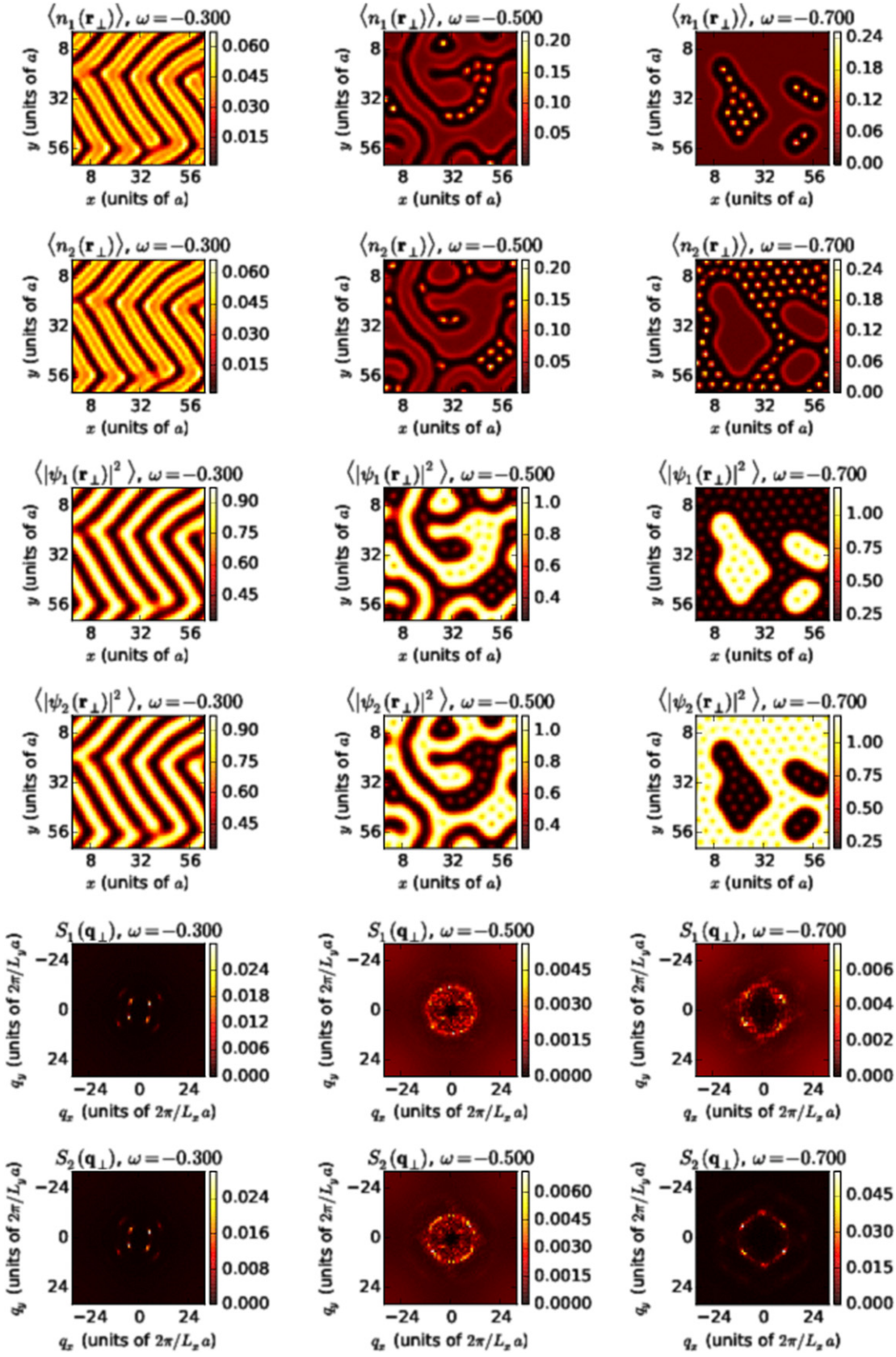

Figure 9. Tableaux showing detailed real space and reciprocal space pictures of the transition from Region II to Region III. The parameter ω is varied between each column, $\omega \in \{-0.300, -0.500, -0.700\}$, while the inverse temperature is fixed, $\beta = 1.2$. Each row shows, from top to bottom, averaged vortex densities of each component, $\langle n_i(\mathbf{r}_\perp)\rangle$, averaged amplitude densities of each component, $\langle |\psi_i(\mathbf{r}_\perp)|\rangle$, and vortex structure functions of each component, $S_i(\mathbf{q}_\perp)$. The first column shows a configuration close to a pure Region II configuration, the second column is a configuration from the highly metastable crossover region, while the last column shows a configuration close to a pure Region III configuration. Note that we consider both the first and the last column to be in Region II and III, respectively, as they consist of purely of domains with configurations from either region, not a mixture of the two.

depleted density due to the $\mathbb{Z}_2$ -symmetry breaking) remains in the isotropic vortex liquid phase. The phase transition from Region II to Region III, driven by increasing the dominance of inter-component density–density interactions over intra-component density–density interactions, involves at the very least a spontaneous breaking of a $\mathbb{Z}_2$ -symmetry as the two condensate components pass from a nematic state of intercalated lattices of 1D vortex liquids into a mixed state of an isotropic vortex liquid in one component and a hexagonal vortex lattice in the other component. This transition is characterized by a broad regime of metastable states with inhomogeneous phase separation.

Figure 8 suggests that the rotation frequency is much smaller than the second critical frequency Ω_{c2}. A crude estimate for the rotation frequency may be obtained as follows. If the rotation frequency were to be set at upper critical rotation frequency Ω_{c2}, the vortex cores would start overlapping, thus covering the plane perpendicular to the rotation. The actual rotation frequency Ω may thus be estimated in terms of the upper critical rotation as $\Omega/\Omega_{c2} = c$, where c is a numerical factor given by the fraction of the area of the plane perpendicular to the rotation which is covered by vortex cores. Thus, an estimate, based on core size, gives $\Omega \propto 0.1\ \Omega_{c2}$. This puts the system well outside the regime of lowest-Landau level physics. The system is therefore indeed in a regime where it makes sense to talk about vortex-degrees of freedom rather than zeroes of the order parameter as the relevant degrees of freedom. For this rotation frequency, we have found the critical value of ω (one of our interaction parameters) to observe phase IV to be $\omega_c \approx -0.6$. This requires scattering lengths $a_{12}/a_{11} > 1.3$. Since these scattering lengths *a priori* are similar, and can be manipulated with Feshbach resonances, it seems feasible to be able to observe phase IV. In order to see the striped ground states phase II, the requirement is only that $a_{12}/a_{11} > 1$, which certainly seems to be within the realms of possibility.

In this paper we have studied the system in the thermodynamic limit. Nonetheless, the results also yield insights into certain aspects of the physics of finite systems with phase separation of species in which the total numbers of particles are finite and independently conserved. For instance, for conserved total number of particles and in the absence of rotation, a finite two-component system can form a bi-domain in the low temperature state in the parameter regime we have considered in this paper. In our case, the ground state is a mono-domain. In both cases, however, the system evolves into similar mixed states at increased temperature. Thus, although the thermodynamic limit calculations provide insights into the phases and phase transitions in the systems, it also calls for further investigation of finite systems of this kind in the presence of a trap.

Acknowledgments

PNG was supported by NTNU and the Research Council of Norway. EB was supported by the Knut and Alice Wallenberg Foundation through a Royal Swedish Academy of Sciences Fellowship, by the Swedish Research Council grants 642-2013-7837, 325-2009-7664, and by the National Science Foundation under the CAREER Award DMR-0955902, AS was supported by the Research Council of Norway, through Grants 205591/V20 and 216700/F20, as well as European Science Foundation COST Action MPI1201. This work was also supported through the Norwegian consortium for high-performance computing (NOTUR).

References

[1] Myatt C J, Burt E A, Ghrist R W, Cornell E A and Wieman C E 1997 *Phys. Rev. Lett.* **78** 586
[2] Modugno G, Modugno M, Riboli F, Roati G and Inguscio M 2002 *Phys. Rev. Lett.* **89** 190404
[3] Thalhammer G, Barontini G, de Sarlo L, Catani J, Minardi F and Inguscio M 2008 *Phys. Rev. Lett.* **100** 210402
[4] McCarron D J, Cho H W, Jenkin D L, Köppinger M P and Cornish S L 2011 *Phys. Rev.* A **84** 011603
[5] Raithel G, Birkl G, Kastberg A, Phillips W D and Rolston S L 1997 *Phys. Rev. Lett.* **78** 630
[6] Müller-Seydlitz T, Hartl M, Brezger B, Hänsel H, Keller C, Schnetz A, Spreeuw R J C, Pfau T and Mlynek J 1997 *Phys. Rev. Lett.* **78** 1038
[7] Hamann S E, Haycock D L, Klose G, Pax P H, Deutsch I H and Jessen P S 1998 *Phys. Rev. Lett.* **80** 4149
[8] Friebel S, D'Andrea C, Walz J, Weitz M and Hänsch T W 1998 *Phys. Rev.* A **57** R20
[9] Guidoni L and Verkerk P 1998 *Phys. Rev.* A **57** R1501
[10] Catani J, de Sarlo L, Barontini G, Minardi F and Inguscio M 2008 *Phys. Rev.* A **77** 011603
[11] Lin Y-J, Compton R L, Jimnez-Garca K, Porto J V and Spielman I B 2009 *Nature* **482** 628
[12] Lin Y-J, Compton R L, Perry A R, Phillips W D, Porto J V and Spielman I B 2009 *Phys. Rev. Lett.* **102** 130401
[13] Galitski V and Spielman I B 2013 *Nature* **494** 49
[14] Kasamatsu K, Tsubota M and Ueda M 2003 *Phys. Rev. Lett.* **91** 150406
[15] Kasamatsu K, Takeuchi H, Tsubota M and Nitta M 2013 *Phys. Rev.* A **88** 013620
[16] Tojo S, Taguchi Y, Masuyama Y, Hayashi T, Saito H and Hirano T 2010 *Phys. Rev.* A **82** 033609
[17] Celabrese P, Pelissetto A and Vicari E 2002 *Phys. Rev.* B **67** 054505
[18] Ceccarelli G, Nespolo J, Pelissetto A and Vicari E 2015 arXiv:cond-mat/1506.04895
[19] Cipriani M and Nitta M 2013 *Phys. Rev.* A **88** 013634
[20] Catelani G and Yuzbashyan E A 2010 *Phys. Rev.* A **81** 033629
[21] Mueller E J and Ho T-L 2002 *Phys. Rev. Lett.* **88** 180403
[22] Filatrella G, Malomed B A and Salerno M 2014 *Phys. Rev.* A **90** 043629
[23] Kuopanportti P, Huhtamäki J A M and Möttönen M 2012 *Phys. Rev.* A **85** 043613

[24] Battye R A, Cooper N and Sutcliffe P M 2002 *Phys. Rev. Lett.* **88** 080401
[25] Kasamatsu K and Tsubota M 2009 *Phys. Rev.* A **79** 023606
[26] Papp S B, Pino J M and Wieman C E 2008 *Phys. Rev. Lett.* **101** 040402
[27] Galteland P N, Babaev E and Sudbø A 2015 *Phys. Rev.* A **91** 013605
[28] Metropolis N, Rosenbluth A W, Rosenbluth M N, Teller A H and Teller E 1953 *J. Chem. Phys.* **21** 1087
[29] Hastings W K 1970 *Biometrika* **57** 97
[30] Matsumoto M and Nishimura T 1998 *ACM Trans. Model. Comput. Simul.* **8** 3
[31] Ferrenberg A M and Swendsen R H 1989 *Phys. Rev. Lett.* **63** 1195
[32] Berg B A 1992 *Comput. Phys. Commun.* **69** 7
[33] Bojesen T A, Babaev E and Sudbø A 2014 *Phys. Rev.* B **89** 104509
[34] Bojesen T A, Babaev E and Sudbø A 2013 *Phys. Rev.* B **88** 220511
[35] Dahl E K, Babaev E, Kragset S and Sudbø A 2008 *Phys. Rev.* B **77** 144519
[36] Herland E V, Babaev E and Sudbø A 2010 *Phys. Rev.* B **82** 134511
[37] Kuklov A, Prokofev N, Svistunov B and Troyer M 2006 *Ann. Phys., NY* **321** 1602
[38] Kragset S, Smørgrav E, Hove J, Nogueira F S and Sudbø A 2006 *Phys. Rev. Lett.* **97** 247201
[39] Kuklov A, Prokof'ev N and Svistunov B 2005 arXiv:cond-mat/0501052
[40] Kuklov A, Prokof'ev N and Svistunov B 2004 *Phys. Rev. Lett.* **92** 030403
[41] Sellin K A H and Babaev E 2013 *Phys. Rev.* E **88** 042305
[42] Garaud J and Babaev E 2015 *Phys. Rev.* B **91** 014510